Published in final edited form as:
J Mol Cell Cardiol. 2014 September ; 74: 318–329. doi:10.1016/j.yjmcc.2014.06.011.

Hypertrophic Cardiomyopathy Associated Lys104Glu Mutation in the Myosin Regulatory Light Chain Causes Diastolic Disturbance in Mice

Wenrui Huang[1], **Jingsheng Liang**[1], **Katarzyna Kazmierczak**[1], **Priya Muthu**[1], **Divya Duggal**[2], **Gerrie P. Farman**[3], **Lars Sorensen**[4], **Iraklis Pozios**[4], **Theodore P. Abraham**[4], **Jeffrey R. Moore**[3], **Julian Borejdo**[2], and **Danuta Szczesna-Cordary**[1,*]

[1]University of Miami, Miller School of Medicine, Miami, FL, 33136

[2]University of North Texas Health Science Center, Fort Worth, TX, 76107

[3]Boston University School of Medicine, Boston, MA, 02118

[4]Johns Hopkins University School of Medicine, Baltimore, MD, 21205

Abstract

We have examined, for the first time, the effects of the familial hypertrophic cardiomyopathy (HCM)- associated Lys104Glu mutation in the myosin regulatory light chain (RLC). Transgenic mice expressing the Lys104Glu substitution (Tg-MUT) were generated and the results compared to Tg-WT (wild-type human ventricular RLC) mice. Echocardiography with pulse wave Doppler in 6 month-old Tg-MUT showed early signs of diastolic disturbance with significantly reduced E/A transmitral velocities ratio. Invasive hemodynamics in 6 month-old Tg-MUT mice also demonstrated a borderline significant prolonged isovolumic relaxation time (Tau) and a tendency for slower rate of pressure decline, suggesting alterations in diastolic function in Tg-MUT. Six month-old mutant animals had no LV hypertrophy; however, at >13 months they displayed significant hypertrophy and fibrosis. In skinned papillary muscles from 5-6 month-old mice a mutation induced reduction in maximal tension and slower muscle relaxation rates were observed. Mutated cross-bridges showed increased rates of binding to the thin filaments and a faster rate of the power stroke. In addition, ~2-fold lower level of RLC phosphorylation was observed in the mutant compared to Tg-WT. In line with the higher mitochondrial content seen in Tg-MUT hearts, the MUT-myosin ATPase activity was significantly higher than WT-myosin, indicating increased energy consumption. In the *in vitro* motility assay, MUT-myosin produced higher actin sliding velocity under zero load, but the velocity drastically decreased with applied load in the MUT vs.

*Corresponding author: Danuta Szczesna-Cordary, PhD Professor of Molecular and Cellular Pharmacology University of Miami Miller School of Medicine 1600 NW 10th Ave Miami, FL 33136 dszczesna@med.miami.edu Phone:+0013052432908 Fax: +0013052434555.

Disclosure statement
The authors declare that they have no conflict of interest.

WT myosin. Our results suggest that diastolic disturbance (impaired muscle relaxation, lower E/A) and inefficiency of energy use (reduced contractile force and faster ATP consumption) may underlie the Lys104Glu-mediated HCM phenotype.

Keywords

Hypertrophic cardiomyopathy (HCM); transgenic mice; myosin regulatory light chain; mutation; contractile force; echocardiography

1. Introduction

Cardiac muscle contraction relies on the ATP-dependent interaction of the myosin heads (S1) with actin to produce the sliding filament movement and generate force [1]. Myosin S1 consists of two major structural domains: the motor domain with the actin and ATP binding sites, and the lever arm domain composed of an 8.5 nm long α-helical region of the myosin heavy chain (MHC) containing the sites of attachment for the myosin regulatory (RLC) and essential (ELC) light chains [2]. Both light chains support the structure and function of the myosin lever arm and contribute to the power stroke and force generation processes. It is therefore very likely for genetically mutated light chains to induce detrimental effects on the mechanical properties of the lever arm and to compromise the ability of myosin motor to produce force and muscle contraction [3].

The myosin RLC is a member of the EF-hand Ca^{2+} binding protein family, which includes troponin C and calmodulin. Unlike other EF-hands, RLC contains only one Ca^{2+} binding EF-hand domain with the helix-loop-helix motif, which can be occupied by either Ca^{2+} or Mg^{2+} [4] (Fig. 1A). It has been postulated that during cardiac muscle contraction, this site could act as a delayed Ca^{2+} buffer helping the sarcoplasmic reticulum in sequestering Ca^{2+} during diastole [5, 6]. Another functionally important domain of the RLC is the myosin light chain kinase (MLCK)-dependent phosphorylation site at serine 15 (Ser15) (Fig. 1A). Numerous studies have shown that RLC phosphorylation can regulate the inotropic state of the heart and therefore any change in RLC phosphorylation during muscle contraction is expected to cause abnormal heart performance, presumably through morphological and/or functional alterations, e.g. change in force, myofilament calcium sensitivity, ATPase activity, etc. [7-9]. Consistent with this notion, it was shown that RLC phosphorylation *in vivo* may prevent the development of the hypertrophic phenotype [10]. Thus, both regions of RLC, the calcium binding site and the phosphorylation domain are important regulators of RLC function and any mutations located in these sites or their vicinity are expected to affect cardiac muscle contraction.

Dominant mutations in *MYL2* (Fig. 1A) encoding the human ventricular RLC are known to cause familial hypertrophic cardiomyopathy (HCM), a complex and heterogeneous disorder with extensive diversity in the course of the disease, age of onset, severity of symptoms and risk for sudden cardiac death (SCD) [11]. HCM is the most common cause of SCD among young individuals and competitive athletes [12]. Recent genetic studies have revealed that mutations in *MYL2* are more common than previously reported (for review see [13, 14]) and in just the past few years, new *MYL2* mutations have been identified [15, 16], with some

detected multiple times and in different ethnic populations (Fig. 1A) [17, 18]. This report focuses on the Lysine 104→Glutamic acid mutation in *MYL2* (Lys104Glu) identified in a Danish family, with the proband diagnosed with HCM at the age of 17 years [18, 19]. At 35 years, he had pronounced septal hypertrophy and an inverted transmitral flow pattern indicating diastolic filling abnormalities [19]. However, the proband and his two family members were also positive for a splice acceptor site mutation in *MYL2* making the target allele for HCM ambiguous. Two family members who exclusively carried the Lys104Glu mutation did not have clinical phenotypes consistent with HCM further complicating the causative role of the Lys104Glu mutation in HCM [18, 19].

In this report we aimed to mechanistically elucidate the effect of the Lys104Glu substitution on heart function and verify whether the mutated *MYL2* allele triggers HCM in mice. For this purpose, we have generated the α-MHC driven transgenic (Tg) mouse model specifically expressing the Lys104Glu-mutated human ventricular RLC (Fig. 1B) in the mouse heart (Tg-MUT). All results were compared to Tg-WT (wild-type) expressing the full length and non-mutated human ventricular RLC. Cardiac muscle preparations of increasing levels of complexity, from myosin through myofibrils and small muscle strips to the intact heart were subjected to morphological and functional assessments. Our results in mice confirm the causative role of the Lys104Glu mutation in the development of HCM. We found changes in diastolic function and inefficient energy usage in young adult mice and a pronounced cardiac hypertrophy in senescent animals. Myosin RLC phosphorylation in Tg-MUT myocardium was significantly reduced compared to Tg-WT hearts suggesting that the mutation-mediated inhibition of RLC phosphorylation may contribute to the development of HCM in mice.

2. Methods

Detailed materials and methods are outlined in the supplement.

2.1. Generation and characterization of transgenic Lys104Glu (Tg-MUT) mice. All animal studies were conducted in accordance with institutional guidelines. We have produced transgenic mice expressing the Lys104Glu-mutated RLC and the results were compared to previously generated Tg-WT mice expressing the human ventricular RLC (GenBank accession no. **P10916**) [6]. Transgenic protein and mRNA expression, RLC phosphorylation and mitochondrial content are described in detail in the supplement and in [20].

2.2. *In vivo* study. Echocardiography and invasive hemodynamics, histopathology and electron mictroscopy examinations were performed as reported previously [20-23] and described in detail in the supplement.

2.3. Studies on skinned papillary muscle strips (force-pCa relationship, relaxation kinetics, passive tension) were performed as in [20, 23].

2.4. Fluorescence polarization study was performed as in [24].

2.5. Actin-activated Tg-mouse myosin ATPase activity and **2.6. *In vitro* motility assays** were performed as in [20, 25].

3. Results

3.1. Transgenic Lys104Glu-RLC mouse model

To study the effects of the Lys104Glu mutation in a mouse model we have successfully produced multiple lines of Tg-MUT mice expressing high levels of the mutant RLC in mouse hearts (Fig. 1B). A substantial difference in gel mobility was observed between Tg human ventricular RLC (WT or Lys104Glu) and the endogenous mouse atrial RLC (GenBank accession no. **Q9QVP4**: MW 19.450 kDa) (Fig. 1B upper panel) making quantification of the transgene expression in atrial preparations useful and efficient. On the other hand no differential gel mobility due to very little difference in molecular weights was observed between endogenous mouse (GenBank accession no. **P51667**: MW 18,864 kDa) and Tg human (GenBank accession no. **P10916**: MW 18,789 kDa) ventricular RLC (Fig. 1B, lower panel). The following levels of mutant expression were achieved: Tg-MUT L2: ~95% , L3: ~97% and L7: ~99% (Fig. 1B). There was no difference in protein expression assessed in the myofibrils prepared from atria or ventricles vs. atrial or ventricular extracts from Tg-mice indicating that all expressed MUT proteins were incorporated into the myofilaments. The mRNA expression profile assessed by quantitative real-time PCR in all three lines of Tg-MUT mice is shown in Fig. 1C. No significant differences in *MYL2* content between atria and ventricles were observed for all tested transgenic lines. NTg atria and ventricles were used as controls and showed no expression of the human *MYL2* gene in mice (Fig. 1C). All three Tg-MUT lines together with Tg-WT L2 [6] were used in the functional assays presented below.

3.2. Mutation induced diastolic disturbance in mice

Diastolic function was assessed using pulse-wave Doppler images of the transmitral filling pattern with the early transmitral filling wave followed by the late filling wave due to atrial contraction and by TDI. Even though, the mutant mice displayed no sign of LV hypertrophy at 6-month with similar anterior and posterior walls and LV-mass, they showed signs of diastolic disturbance with significantly lower E/A-ratios (Fig. 2 and Table 1). A slightly prolonged deceleration time was observed in the mutant compared with WT but the difference between the groups was not statistically significant ($P>0.05$). The TDI-measurements including e’ and E/e’ were similar between Tg-WT and Tg-MUT indicating no effect on LV filling pressure and therefore suggesting mild diastolic dysfunction in the mutant if classified according to human guidelines [26].

Invasive hemodynamics evaluation of 6-month old mutant vs. control mice showed preserved systolic function in Tg-MUT compared to Tg-WT mice. However, we found indications of impaired diastolic function in the mutant mice represented by: 1) Tau (time of isovolumic relaxation), which was 58% longer in Tg-MUT compared to Tg-WT, and 2) dp/dtmin, which was reduced in the mutant showing a slower rate of pressure decline (Table 1). Due to the small number of examined mice the differences between the groups were borderline significant (Table 1).

3.3. Cardiac hypertrophy in senescent mutant mice

As reported by Andersen et al., the 35 year old proband carrying the Lys104Glu mutation had pronounced septal hypertrophy at the time of screening but was diagnosed with HCM at the age of 17 years [19]. We have not observed any morphological HCM features in 6 month-old Tg-MUT mice (Table 1) but the hypertrophic phenotype was evident in senescent (aged >13 months) mice (Table 2). Old Tg-MUT and Tg-WT mice had similar body weights, but the mutant displayed significant hypertrophy of both anterior and posterior wall and consequently a ~1.6-fold higher LV mass compared to Tg-WT mice. The hypertrophic phenotype in old Tg-MUT animals showed concentric pattern manifested by reduced LV diameter in systole and diastole compared to senescent Tg-WT mice (Table 2). The EF was higher in Tg-MUT compared to Tg-WT mice, indicating that the observed hypertrophy in mutant animals did not compromise their systolic function. The increased EF in HCM is well established [27], but it is mostly due to reduced volumes as observed in our senescent mutant mice (Table 2). In addition, it has been demonstrated that even though HCM patients may have increased EF, they usually show reduced LV function [27, 28]. Consistently with our results (see below), impaired myofilament contractile function was suggested to be the most important mechanism in HCM, accounting for compensatory hypertrophy and diastolic dysfunction, forming two of the hallmarks of the clinical HCM phenotype [29].

3.4. Development of cardiomyopathic phenotype in Tg-MUT mice

Histopatological evaluation of the hearts from mice of different ages: ~ 4 (young), ~8 (intermediate) and ~15 (old) month-old Tg-MUT and Tg-WT showed no major abnormalities and the lack of myofilament disarray in either group of mice (Fig. 3A). However, occurrences of mild fibrosis were noted in 8 month old Tg-MUT animals, which severely intensified in 15 month-old mice compared to Tg-WT hearts (Fig. 3B). Myocardial fibrosis is a hallmark of hypertrophic cardiomyopathy and the activation of profibrotic genetic pathways can take place even before hypertrophic remodeling [30]. Accordingly, gradually increasing fibrotic lesions were seen in the hearts of Tg-MUT animals implying that these changes did precede the development of LV hypertrophy (Fig. 3B). Echocardiography examination of senescent animals confirmed a fully developed hypertrophic phenotype in Tg-MUT vs. Tg-WT mice (Table 2).

To determine whether the Lys104Glu mutation has an effect on sarcomeric structure, we have performed electron microscopy assessment of LV tissue from Tg-MUT vs. Tg-WT mice (Fig. 4A). No significant defects in the sarcomeric ultrastructure were observed in the myocardium of ~6 month old Tg-MUT mice compared to age and gender matched Tg-WT controls and the cardiac muscle of both groups of mice demonstrated normally arranged and aligned in series sarcomeres (Fig. 4A). However, in contrast to Tg-WT myocardium, the mutant hearts displayed visibly abundant mitochondria with the preserved overall architecture. To quantify the mitochondrial content we have run SDS-PAGE on the heart extracts and probed for the mitochondrial protein VDAC (porin). The myosin ELC was used as a loading control. Fig. 4B, upper panel shows a representative Western blot of heart samples from 4 and 14 month-old Tg-MUT mice (lanes 2 and 4) compared to samples from 4 and 14 month-old Tg-WT mice (lanes 1 and 3). At least two mice per group were tested. Both young and old Tg-MUT mice showed a significantly higher mitochondrial VDAC

content compared to age matched Tg-WT controls. About 1.7-fold difference between Tg-MUT and Tg-WT of young and old mice was monitored ($P<0.05$) (Fig. 4B, lower panel). These data indicate that more mitochondria might be recruited by Tg-MUT vs. Tg-WT hearts suggesting their higher energetic demands during force generation and cardiac muscle contraction.

A direct correlation between compromised RLC phosphorylation and the development of cardiomyopathic phenotype was noted in our previous studies on Tg-RLC mouse models of HCM [21, 31], and was also reported by Sheikh et al. [32]. Therefore, we have examined the hearts of Tg-MUT mice for a mutation-induced effect of myosin RLC phosphorylation. Fig. 4C demonstrates ~2.2-fold reduction in endogenous RLC phosphorylation in young Tg-MUT mice compared to young Tg-WT mice, and ~1.7-fold decrease in old Tg-MUT compared to old Tg-WT. Phosphorylation was determined by SDS-PAGE of myofibrils (n=13 runs for each group of mice) isolated from left ventricles of rapidly frozen 3 and 17 month-old Tg-MUT (lanes 2 and 4) vs. 3 and 18 month-old Tg-WT (lanes 1 and 3) hearts (Fig. 4C, upper panel). The extent of RLC phosphorylation was evaluated using our generated phospho-specific RLC antibody [20], which recognizes the phosphorylated form of the RLC (lane 6). As observed previously [20], there was no reaction with the unphosphorylated RLC (lane 5). Total RLC protein was probed with the CT-1 antibody as described in our earlier publications [6, 20, 23, 31]. This result confirms our earlier observations of compromised RLC phosphorylation in cardiomyopathic myocardium, especially in those mouse models which show strong HCM phenotypes [21, 31].

3.5. Assessment of contractile function in skinned papillary muscle strips from Tg-MUT vs. Tg-WT mice

Measurements of steady-state force generation were performed in skinned papillary muscle strips from 5-6 month old male and female Tg-MUT and Tg-WT mice (5-7 mice per group). A significant reduction in maximal isometric force was observed in Tg-MUT compared with Tg-WT mice ($P<0.01$) (Fig. 5A). The values of tension per cross-sectional area of muscle (in kN/m^2 ± SEM) were: Tg-MUT: 36.8±0.7 vs. Tg-WT: 52.8±0.78. The average diameter of muscle strip (in μm ± SEM) was 102±2 for Tg-MUT and 97±2 for WT (Fig. 5A). There was a slight but not statistically significant increase in pCa_{50} of the force-pCa dependence: 5.72±0.01(SEM) for Tg-MUT and 5.70±0.01(SEM) for Tg-WT (Fig. 5B). Likewise no significant differences in the Hill coefficient were seen between the groups: 2.55±0.11 (SEM) for Tg-MUT and 2.59±0.07 (SEM) for Tg-WT (Fig. 5B). All these data were derived from n=66 papillary muscle strips from Tg-MUT and n=58 strips from Tg-WT hearts (Fig. 5).

Since a phenotype of diastolic filling abnormalities was reported in Lys104Glu-positive patients, we further assessed the muscle relaxation kinetics in skinned papillary muscle strips from Tg-MUT and Tg-WT mice (three 7 month-old mice per group). A significant decrease in the muscle relaxation rate k_1 was observed in Tg-MUT vs. Tg-WT myocardium (Fig. 5C, $P<0.01$). The relaxation rate values (in s^{-1} ± SEM) were: k_1=15.5±0.6 for Tg-MUT (n=36 strips) compared to k_1=23.7±1.2 for Tg-WT (n=32 strips). The amplitudes of k_1 were 0.73±0.02 for Tg-MUT and 0.83±0.07 for Tg-WT. The fit to a double exponential

curve yielded the slow k_2 rates of ~1.1 for Tg-MUT and ~0.4 for Tg-WT with amplitudes of ~0.3. The k_2 rates most likely represent a small population of cross-bridges at a different isomerization state compared to the larger population of the faster dissociating cross-bridges [33]. These results indicated a mutation-induced impairment in the muscle relaxation kinetics suggesting that Tg-MUT hearts might be prone to diastolic disturbance.

Diastolic dysfunction is often associated with alterations in muscle stiffness, and therefore we also proceeded to measure the level of passive tension (at pCa 8) in response to muscle stretch using two 6 month-old mice per group (Fig. 5D). The following values of passive tension (in $kN/m^2 \pm$ SEM) were measured as a function of muscle stretch: Tg-MUT: 10%, 1.45±0.21; 20%, 5.17±0.37; 30%, 10.81±0.50; and 40%, 18.47±0.40 (n=25 strips) compared to Tg-WT: 10%, 1.14 ±0.18; 20%, 4.07±0.25; 30%, 8.17±0.40; and 40% 13.88±0.66 (n=19 strips). The P value between Tg-MUT and Tg-WT groups was <0.001 as determined by ANOVA for repeated measurements (Fig. 5D). In conclusion, Tg-MUT preparations displayed significantly increased levels of passive tension compared to Tg-WT, suggesting an increase in muscle stiffness in the mutant myocardium.

3.6. The effect of the Lys104Glu mutation at the level of single myosin cross-bridges

Using single molecule detection, we aimed to find out whether the effect of mutation seen in the whole muscle could also be observed at the level of individual myosin cross-bridges. The cross-bridges in myofibrils prepared from 3-5 hearts per group were inefficiently exchanged with the fluorescent dye SeTau covalently coupled to ELC. To prevent shortening and at the same time to avoid cross-bridges from executing their power generating cycle, they were cross-linked with zero-length, water soluble cross-linker EDC. The fluorescent cross-bridges were observed under confocal microscope. Inefficient fluorescent labeling combined with minimal confocal volume allowed us to observe ~20 myosin molecules. To assess the rate at which cross-bridges were rotating during contraction, polarization anisotropy was measured (see below). Fig. 6A shows a typical image of Tg-MUT myofibril during relaxation. The gray circle pointed to by an arrow represents the observation volume. It contains ~20 fluorescent myosin molecules (and ~40,000 non-fluorescent myosin molecules). The fluorescent signal was divided into two orthogonal components and then fluorescence anisotropy, which is known to be an accurate measure of the cross-bridge orientation, was computed. Autocorrelation function (ACF) of fluctuations of anisotropy was then calculated. The fluctuations were large (~20%) due to limited (only ~20) number of observed molecules.

The kinetics rates were estimated from ACF by adopting a conventional model of the cross-bridge action, schematically shown in Fig. 6B. The model predicts that the lever arm of a cross bridge has different conformations in different contractile states. Thus, the intensity of fluorescent light fluctuates around the equilibrium value. Every inflection in ACF corresponds to a specific kinetic step. The first step of this model is a dissociation of myosin head (M) from the thin filament actin (A) by binding of ATP (T). ATP is hydrolyzed to ADP (D) and Phosphate (P). Myosin and the products of hydrolysis are free to rotate in the myofilament space, so the anisotropy is low. Next, a cross-bridge binds with a rate k_1 to actin to assume a pre-power stroke state, AMDP. It is in a weakly bound and partially

immobilized state. Myosin power-stroke, occurring at a rate k_2, is initiated by dissociation of the hydrolysis products. Cross-bridges now become strongly bound to actin. The rate k_3 is a rate of transition to a high anisotropy AMT* state reflecting a ternary "rigor-like" state in which anisotropy is the largest as M is still attached to A (Fig. 6B). Cross-bridge dissociation occurs only after this step. Kinetic constants estimated from ACF of 28 experiments per group are as follows (in s^{-1} ± SD): k_1 (rate of cross-bridge binding): 205.9±93.7 for Tg-WT and 779.1±572.1 for Tg-MUT. The −573.2 difference in k_1 is statistically significant ($t = -4.745$, $P<0.001$ with 50 degrees of freedom); k_2 (rate of power stroke): 0.617±0.496 for Tg-WT and 1.162±1.198 for Tg-MUT. The −0.545 difference in k_2 is statistically significant ($t = -2.091$, $P=0.041$ with 53 degrees of freedom); k_3 (rate of transition to "rigor-like" state): 0.689±0.499 for Tg-WT and 0.300±0.242 for Tg-MUT. The +0.389 difference in k_3 is also statistically significant ($t = 3.809$, $P=0.001$ with 53 degrees of freedom). In summary, the Lys104Glu mutation increased the rate of cross-bridge binding (k_1) and the rate of execution of the power stroke (k_2) and decreased the rate of transition to a "rigor-like" state. The fact that k_3 is smaller in the mutant suggests that cross-bridges stay attached longer to actin implying that the relaxation would take a longer time to be completed.

3.7. The effect of Lys104Glu on myosin ATPase and its force production capacity

Two age groups (~6 month old and ~11 month old) of mice were used to obtain myosin from Tg-MUT and Tg-WT mice. No age-dependent differences within each group were noted in solution experiments using various batches of myosin (data not shown). Actin-activated myosin ATPase activity was plotted as a function of F-actin concentration (in μM) with data points expressed as average ± SEM of n=13-16 experiments. The data were fitted to the Michaelis-Menten equation yielding the V_{max} and K_m parameters. The V_{max} represents the rate constant of the detachment step and the transition from the weakly (A·M·ATP↔A·M·ADP·Pi) to strongly (A·M·ADP↔A·M) bound cross bridges. The K_m determines the concentration of actin needed to produce half of the activation of the myosin heads and stands for the binding affinity of actin to myosin. Fig. 7A shows a significant ($P<0.01$) increase in V_{max} in Tg-MUT mice (0.62±0.03 s^{-1}, n=13) compared to Tg-WT (0.27±0.04 s^{-1}, n=16). The K_m values were not different between Tg-WT (5.0±2.4 μM, n=16) and Tg-MUT (6.6±0.9 μM, n=13) mice. These results demonstrate that while the Lys104Glu mutation does not change the affinity of binding (no change in K_m), it facilitates the detachment state and thus produces the quicker ATPase cycle (increase in V_{max}) compared to WT.

In order to assess the acto-myosin interaction in the presence of a frictional load, the *in vitro* motility assays were performed in the presence of α-actinin, a low affinity actin binding protein. The use of α-actinin was to slow down the actin filament motion and served as an indicator of the force generation capacity of myosin molecules. Compared with WT, Lys104Glu-myosin produced a higher actin sliding velocity under no load (no α-actinin added) (Fig. 7B) without a change in the % motile filaments (Fig. 7C). Increased V_{max} observed in the ATPase assays could also be attributed to a contribution of attachment to velocity as described by others [34, 35] and observed in this report. Both actin sliding velocity and fraction of motile filaments observed with MUT-myosin decreased drastically

with increasing amounts of α-actinin with actin filament velocities driven by MUT-myosin falling below WT values. The reduction in velocity under light and intermediate loads (2-4 μg/ml α-actinin added) is consistent with the reduced muscle relaxation rate determined in Tg-MUT skinned muscle strips (Fig. 5C). Furthermore, a mutation-induced higher sensitivity of actin filament velocity to load indicates that the Lys104Glu mutation inhibits myosin force production. This result is consistent with reduced steady state force observed in Tg-MUT vs. Tg-WT skinned muscle preparations (Fig. 5A), and suggests that the Lys104Glu mutation may affect, at least in part, the myosin's force production capacity.

4. Discussion

The Lys104Glu mutation in the myosin RLC has been linked to familial hypertrophic cardiomyopathy [19], but the molecular mechanism underlying its effect on heart function is not known. Limited clinical reports that identified this new Lys104Glu – *MYL2* variant also revealed a paternally inherited splice site mutation present in the Lys104Glu positive proband, confounding the genetic basis of HCM in the family [18, 19]. In this study, we aimed to evaluate the functional consequences of Lys104Glu using transgenic mice (Tg-MUT) expressing the mutant RLC in the heart. The *in vivo* and *in vitro* phenotypes associated with Lys104Glu-RLC were compared to those observed in our previously generated Tg-WT mice [6], expressing the WT human ventricular RLC.

Echocardiography assessment of Tg-MUT mice showed no sign of LV hypertrophy at 6 months with similar anterior and posterior walls and LV-mass. However, they displayed early signs of diastolic dysfunction with a significantly reduced E/A ratio and a borderline prolonged deceleration time compared to Tg-WT mice (Fig. 2 and Table 1). Mature animals (>13 months of age) from both groups had similar body weights but Tg-MUT demonstrated significant hypertrophy of concentric phenotype manifested by reduced dimensions of the LV cavity in systole and diastole and a higher LV mass compared to Tg-WT mice (Table 2). Cardiac hypertrophy observed in mature Tg-MUT mice did not compromise their EF, which was actually higher than in Tg-WT mice (Table 2). This observation however is not unexpected and consistent with human studies monitoring a significantly reduced LV function with a preserved or augmented EF in HCM patients [27, 28]. In accord with echocardiography results, histopathology evaluation demonstrated a mild to severe fibrosis in Tg-MUT hearts (Fig. 3B), another characteristic feature of HCM [30]. Hence, the *in vivo* and histological phenotypes observed in Tg-MUT mice strongly support the causative role of the Lys104Glu mutation in the RLC in the development of HCM in mice. Noteworthy, in line with the fibrotic lesions observed in Tg-MUT hearts, the passive tension results imply a mutation induced increase in passive stiffness in Tg-MUT mice compared to Tg-WT. The latter result suggests potential diastolic filling abnormalities in Tg-MUT mice, the phenotype observed in the Lys104Glu-positive proband [19]. The tendency for longer isovolumic relaxation time (Tau) and a significantly decreased E/A ratio observed in Tg-MUT mice (Table 1), suggests a mutation induced diastolic disturbance phenotype.

Given the unique position of the RLC within the lever arm domain of the myosin head [2], one can understand why a structural change brought about by the lysine residue to glutamic acid substitution leads to alterations in cross-bridge function and somewhat abnormal

myosin ATPase cycling kinetics. As we observed in Fig. 7A, the ATPase activity of the mutant myosin was significantly higher than that of the WT. The V_{max} of actin activated myosin ATPase can be determined by two parameters, the cross bridge cycling rate and the number of myosin cross bridges participating in the cycle. The higher V_{max} noted for MUT-myosin suggests that either myosin cross bridge cycling rates were augmented or there were more MUT vs. WT cycling cross-bridges interacting with actin. Consistently, actin sliding velocity, V_{actin} was increased at low loads for MUT when compared to WT (Fig. 7B), while on the other hand, maximal steady state force was significantly lower in the mutant compared with WT controls (Fig. 5A). Therefore, an increase in MUT-myosin cycling rates seems more likely to be responsible for the elevated V_{max}.

Although the mutant myosin exhibits a higher unloaded V_{actin} in the *in vitro* motility assay, actin sliding velocity in the presence of α-actinin-induced frictional load is decreased in the MUT compared to WT myosin (Fig. 7BC) suggesting that the Lys104Glu mutation may affect, at least in part, myosin force production capacity. The ability of myosin to contract against load is crucial to its function in the heart. The inverse relationship between load and contraction velocity has long been recognized to represent the load dependence of actomyosin biochemical transitions and the economy of tension generation [36]. The Lys104Glu-induced disruptions in sensitivity of myosin to exogenous load may lead to inefficient ATP utilization during loaded filament sliding. A similar disruption of load-dependent myosin mechanochemistry has been associated with other RLC-HCM mutations, Asn47Lys and Arg58Gln [3], suggesting a common mechanism for the effects of RLC mutations on myosin strain dependent biochemistry. Taken together, the higher ATP consumption, altered load dependence, and a lower force generated by Tg-MUT hearts may suggest low efficiency of contraction in the mutant. In line with this, the EM results showed more mitochondria recruited by Tg-MUT myocardium compared to Tg-WT (Fig. 4AB), confirming higher energy demands in the mutant hearts.

Phosphorylation of myosin RLC has been shown by many to regulate the multifaceted protein-protein interactions and fine-tune cardiac muscle contraction [9, 37]. Reduced RLC phosphorylation was implicated in abnormal heart performance and cardiac disease [32, 38, 39]. Therefore, we pursued to determine the effect of the Lys104Glu mutation on the level of RLC phosphorylation in Tg-MUT vs. Tg-WT myocardium. We hypothesized that the mutation-induced inhibition in myosin phosphorylation may contribute to the Lys104Glu - mediated development of HCM. Our result of ~2-fold lower level of RLC phosphorylation observed in the hearts of young and old Tg-MUT vs. age matched Tg-WT mice (Fig. 4C) supports this hypothesis and is consistent with our earlier data showing compromised RLC phosphorylation that occurred concurrently with reduced maximal tension in other RLC models of HCM [21, 31, 40]. It is therefore plausible that a mutation-induced inhibition of RLC phosphorylation in Tg-MUT mice contributes to a diminished level of maximal steady state force and slower muscle relaxation kinetics (Fig. 8). These molecular events trigger diastolic disturbance in Tg-MUT mice further manifested by significantly lower E/A transmitral velocities ratio and borderline prolonged Tau (Table 1, Fig. 8). In addition to diastolic disturbance, inefficiency of energy use indicated by reduced contractile force and faster ATP consumption may underlie the Lys104Glu-mediated HCM phenotype.

5. Conclusions

The current study demonstrates the effects of HCM-associated mutation in the myosin RLC on heart morphology, cardiac function *in vivo* and contractile parameters assessed in cardiac muscle preparations *in vitro*. Our results provide potential mechanisms by which the Lys104Glu mutation may lead to HCM in transgenic mice. As schematically demonstrated in Fig. 8, the Lys104Glu mutation appears to enhance unloaded myosin function (increased ATPase activity and increased V_{actin} at low loads), but as the load increases it significantly reduces myosin performance (reduced isometric force and V_{actin} in the presence of load) indicating a mutation-induced disruption of myosin load-dependent mechanochemistry. The mutation also results in elevated passive tension and slower muscle relaxation. These molecular events further trigger morphological and functional remodeling of the heart manifested by abundant mitochondria, development of fibrosis and altered diastolic indices. These changes are anticipated to result in diastolic disturbance in Tg-MUT mice, which together with inefficiency in energy use and diminished RLC phosphorylation may trigger the development of Lys104Glu-RLC induced heart disease.

Supplementary Material

Refer to Web version on PubMed Central for supplementary material.

Acknowledgments

The authors thank Dr. Yingcai Wang for his help in generating Tg-Lys104Glu constructs, Ana I. Rojas and Michelle Jones for their excellent technical assistance and Janhavi Nagwekar for her contribution to fluorescence polarization experiments. The authors also thank Dr. Hongchang Luo for help in executing the invasive hemodynamics study.

Funding

This work was supported by the National Institutes of Health Grants R01 HL-071778 and HL-108343 (to Danuta Szczesna-Cordary), HL-090786 (to Julian Borejdo and Danuta Szczesna-Cordary) and HL-077280 (to Jeffrey R. Moore).

Abbreviations

ACF	Auto Correlation Function
E/A	Early (E) to late (A) Mitral Inflow Ratio
EDC	1-ethyl-3-[3-(dimethylamino)-propyl]-carbodiimide
EF	Ejection Fraction
ELC	Myosin Essential Light Chain
HCM	Hypertrophic Cardiomyopathy
LV	Left Ventricle
Lys104Glu	Lysine at position 104 substituted by Glutamic Acid
MHC	Myosin Heavy Chain

MLCK	Myosin Light Chain Kinase
MYL2	Human Gene encoding the Ventricular Myosin RLC
NTg	Non-Transgenic
RLC	Myosin Regulatory Light Chain
SCD	Sudden Cardiac Death
Tau	Time of Isovolumic Relaxation TDI
TDI	Tissue Doppler Imaging
Tg-MUT	Transgenic Mutant RLC-Lys104Glu
Tg-WT	Transgenic Wild Type RLC
VDAC	Voltage Dependent Anion Channel

References

1. Geeves MA, Holmes KC. The molecular mechanism of muscle contraction. Adv Protein Chem. 2005; 7l:161–93. [PubMed: 16230112]
2. Rayment I, Rypniewski WR, Schmidt-Base K, Smith R, Tomchick DR, Benning MM, et al. Three-dimensional structure of myosin subfragment-1: a molecular motor. Science. Jul 2; 1993 261(5117): 50–8. [PubMed: 8316857]
3. Greenberg MJ, Kazmierczak K, Szczesna-Cordary D, Moore JR. Cardiomyopathy-linked myosin regulatory light chain mutations disrupt myosin strain-dependent biochemistry. Proc Natl Acad Sci U S A. Oct 5; 2010 107(40):17403–8. [PubMed: 20855589]
4. Szczesna D, Ghosh D, Li Q, Gomes AV, Guzman G, Arana C, et al. Familial hypertrophic cardiomyopathy mutations in the regulatory light chains of myosin affect their structure, Ca^{2+} binding, and phosphorylation. J Biol Chem. Mar 9; 2001 276(10):7086–92. [PubMed: 11102452]
5. Szczesna-Cordary D, Jones M, Moore JR, Watt J, Kerrick WGL, Xu Y, et al. Myosin regulatory light chain E22K mutation results in decreased cardiac intracellular calcium and force transients. FASEB J. Dec 1; 2007 21(14):3974–85. 2007. [PubMed: 17606808]
6. Wang Y, Xu Y, Kerrick WGL, Wang Y, Guzman G, Diaz-Perez Z, et al. Prolonged Ca^{2+} and force transients in myosin RLC transgenic mouse fibers expressing malignant and benign FHC mutations. J Mol Biol. 2006; 361(2):286–99. [PubMed: 16837010]
7. Kamm KE, Stull JT. Signaling to Myosin Regulatory Light Chain in Sarcomeres. J Biol Chem. Mar 25; 2011 286(12):9941–7. 2011. [PubMed: 21257758]
8. Stelzer JE, Patel JR, Moss RL. Acceleration of stretch activation in murine myocardium due to phosphorylation of myosin regulatory light chain. J Gen Physiol. Sep; 2006 128(3):261–72. [PubMed: 16908724]
9. Morano I. Tuning the human heart molecular motors by myosin light chains. J Mol Med. Jul; 1999 77(7):544–55. [PubMed: 10494800]
10. Huang J, Shelton JM, Richardson JA, Kamm KE, Stull JT. Myosin regulatory light chain phosphorylation attenuates cardiac hypertrophy. J Biol Chem. Jul 11; 2008 283(28):19748–56. [PubMed: 18474588]
11. Alcalai R, Seidman JG, Seidman CE. Genetic Basis of Hypertrophic Cardiomyopathy: From Bench to the Clinics. J Cardiovasc Electrophysiol. 2008; 19(1):104–10. [PubMed: 17916152]
12. Maron BJ. The young competitive athlete with cardiovascular abnormalities: causes of sudden death, detection by preparticipation screening, and standards for disqualification. Card Electrophysiol Rev. Feb; 2002 6(1-2):100–3. [PubMed: 11984027]

13. Muthu, P.; Huang, W.; Kazmierczak, K.; Szczesna-Cordary, D. Functional Consequences of Mutations in the Myosin Regulatory Light Chain Associated with Hypertrophic Cardiomyopathy. In: Veselka, J., editor. Cardiomyopathies – From Basic Research to Clinical Management. InTech; Croatia: 2012. p. 383-408.Ch. 17
14. Szczesna D. Regulatory light chains of striated muscle myosin. Structure, function and malfunction. Curr Drug Targets Cardiovasc Haematol Disord. Jun; 2003 3(2):187–97. [PubMed: 12769642]
15. Olivotto I, Girolami F, Ackerman MJ, Nistri S, Bos JM, Zachara E, et al. Myofilament protein gene mutation screening and outcome of patients with hypertrophic cardiomyopathy. Mayo Clin Proc. Jun; 2008 83(6):630–8. [PubMed: 18533079]
16. Santos S, Marques V, Pires M, Silveira L, Oliveira H, Lanca V, et al. High Resolution Melting: improvements in the genetic diagnosis of Hypertrophic Cardiomyopathy in a Portuguese cohort. BMC Med Gen. 2012; 13(1):17.
17. Garcia-Pavia P, Vazquez ME, Segovia J, Salas C, Avellana P, Gomez-Bueno M, et al. Genetic basis of end-stage hypertrophic cardiomyopathy. Eur J Heart Fail. Nov 1; 2011 13(11):1193–201. 2011. [PubMed: 21896538]
18. Andersen PS, Havndrup O, Hougs L, Sorensen KM, Jensen M, Larsen LA, et al. Diagnostic yield, interpretation, and clinical utility of mutation screening of sarcomere encoding genes in Danish hypertrophic cardiomyopathy patients and relatives. Hum Mutat. Mar; 2009 30(3):363–70. [PubMed: 19035361]
19. Andersen PS, Havndrup O, Bundgaard H, Moolman-Smook JC, Larsen LA, Mogensen J, et al. Myosin light chain mutations in familial hypertrophic cardiomyopathy: phenotypic presentation and frequency in Danish and South African populations. J Med Genet. Dec 1.2001 38(12):e43. 2001. [PubMed: 11748309]
20. Kazmierczak K, Muthu P, Huang W, Jones M, Wang Y, Szczesna-Cordary D. Myosin Regulatory Light Chain Mutation Found In Hypertrophic Cardiomyopathy Patients Increases Isometric Force Production in Transgenic Mice. Biochem J. Nov 17; 2012 442(1):95–103. [PubMed: 22091967]
21. Abraham TP, Jones M, Kazmierczak K, Liang H-Y, Pinheiro AC, Wagg CS, et al. Diastolic dysfunction in familial hypertrophic cardiomyopathy transgenic model mice. Cardiovasc Res. Apr 1; 2009 82(1):84–92. 2009. [PubMed: 19150977]
22. Cingolani OH, Kass DA. Pressure-volume relation analysis of mouse ventricular function. Am J Physiol Heart Circ Physiol. Dec; 2011 301(6):H2198–206. [PubMed: 21926344]
23. Szczesna-Cordary D, Guzman G, Zhao J, Hernandez O, Wei J, Diaz-Perez Z. The E22K mutation of myosin RLC that causes familial hypertrophic cardiomyopathy increases calcium sensitivity of force and ATPase in transgenic mice. J Cell Sci. Aug 15.2005 118:3675–83. Pt 16. [PubMed: 16076902]
24. Borejdo J, Szczesna-Cordary D, Muthu P, Metticolla P, Luchowski R, Gryczynski Z, et al. Single molecule detection approach to muscle study: kinetics of a single cross-bridge during contraction of muscle. Methods Mol Biol. 2012; 875:311–34. [PubMed: 22573449]
25. Greenberg MJ, Watt JD, Jones M, Kazmierczak K, Szczesna-Cordary D, Moore JR. Regulatory light chain mutations associated with cardiomyopathy affect myosin mechanics and kinetics. J Mol Cell Cardiol. 2009; 46(1):108–15. [PubMed: 18929571]
26. Redfield MM, Jacobsen SJ, Burnett JC Jr. Mahoney DW, Bailey KR, Rodeheffer RJ. Burden of systolic and diastolic ventricular dysfunction in the community: appreciating the scope of the heart failure epidemic. JAMA. Jan 8; 2003 289(2):194–202. [PubMed: 12517230]
27. Carasso S, Yang H, Woo A, Vannan MA, Jamorski M, Wigle ED, et al. Systolic myocardial mechanics in hypertrophic cardiomyopathy: novel concepts and implications for clinical status. J Am Soc Echocardiogr. Jun; 2008 21(6):675–83. [PubMed: 18187306]
28. Afonso LC, Bernal J, Bax JJ, Abraham TP. Echocardiography in hypertrophic cardiomyopathy: the role of conventional and emerging technologies. JACC Cardiovasc Imaging. Nov; 2008 1(6):787–800. [PubMed: 19356516]
29. Frey N, Luedde M, Katus HA. Mechanisms of disease: hypertrophic cardiomyopathy. Nat Rev Cardiol. Feb; 2012 9(2):91–100. [PubMed: 22027658]

30. Ho CY, Lopez B, Coelho-Filho OR, Lakdawala NK, Cirino AL, Jarolim P, et al. Myocardial fibrosis as an early manifestation of hypertrophic cardiomyopathy. N Engl J Med. Aug 5; 2010 363(6):552–63. [PubMed: 20818890]

31. Kerrick WGL, Kazmierczak K, Xu Y, Wang Y, Szczesna-Cordary D. Malignant familial hypertrophic cardiomyopathy D166V mutation in the ventricular myosin regulatory light chain causes profound effects in skinned and intact papillary muscle fibers from transgenic mice. FASEB J. Nov 5.2009 23:855–65. Epub 2008. [PubMed: 18987303]

32. Sheikh F, Ouyang K, Campbell SG, Lyon RC, Chuang J, Fitzsimons D, et al. Mouse and computational models link Mlc2v dephosphorylation to altered myosin kinetics in early cardiac disease. J Clin Invest. Apr 2; 2012 122(4):1209–21. [PubMed: 22426213]

33. Simnett SJ, Johns EC, Lipscomb S, Mulligan IP, Ashley CC. Effect of pH, phosphate, and ADP on relaxation of myocardium after photolysis of diazo 2. Am J Physiol. Sep.1998 275:H951–60. 3 Pt 2. [PubMed: 9724300]

34. Hooft AM, Maki EJ, Cox KK, Baker JE. An accelerated state of myosin-based actin motility. Biochemistry. Mar 20; 2007 46(11):3513–20. [PubMed: 17302393]

35. Stewart TJ, Jackson DR Jr. Smith RD, Shannon SF, Cremo CR, Baker JE. Actin Sliding Velocities are Influenced by the Driving Forces of Actin-Myosin Binding. Cell Mol Bioeng. Mar 1; 2013 6(1):26–37. [PubMed: 23606917]

36. Fenn WO. A quantitative comparison between the energy liberated and work performed by the isolated sartorus muscle of the frog. J Physiol (Lond). 1923; 58:175–203. [PubMed: 16993652]

37. Davis JS, Hassanzadeh S, Winitsky S, Lin H, Satorius C, Vemuri R, et al. The overall pattern of cardiac contraction depends on a spatial gradient of myosin regulatory light chain phosphorylation. Cell. Nov 30; 2001 107(5):631–41. [PubMed: 11733062]

38. Toepfer C, Caorsi V, Kampourakis T, Sikkel MB, West TG, Leung MC, et al. Myosin regulatory light chain (RLC) phosphorylation change as a modulator of cardiac muscle contraction in disease. J Biol Chem. 2013; 288(19):13446–54. [PubMed: 23530050]

39. Warren SA, Briggs LE, Zeng H, Chuang J, Chang EI, Terada R, et al. Myosin light chain phosphorylation is critical for adaptation to cardiac stress. Circulation. Nov 27; 2012 126(22): 2575–88. [PubMed: 23095280]

40. Muthu P, Kazmierczak K, Jones M, Szczesna-Cordary D. The effect of myosin RLC phosphorylation in normal and cardiomyopathic mouse hearts. J Cell Mol Med. Jun 23; 2012 16(4):911–9. [PubMed: 21696541]

41. Bing W, Knott A, Marston SB. A simple method for measuring the relative force exerted by myosin on actn filaments in the in vitro motility assay: evidence that tropomyosin and troponin increase force in single thin filaments. Biochem J. Sep 15.2000 350:693–9. Pt 3. [PubMed: 10970781]

Highlights

➢ Hypertrophic cardiomyopathy is a serious heart disease affecting young individuals.

➢ Effects of HCM-Lys104Glu mutation in the myosin RLC were tested in transgenic mice.

➢ Mutated hearts displayed diminished contractile force and slower muscle relaxation.

➢ Myosin ATPase and mitochondria were elevated but RLC phosphorylation was reduced.

➢ Inefficiency in energy use and disturbed diastolic function contribute to MUT-HCM.

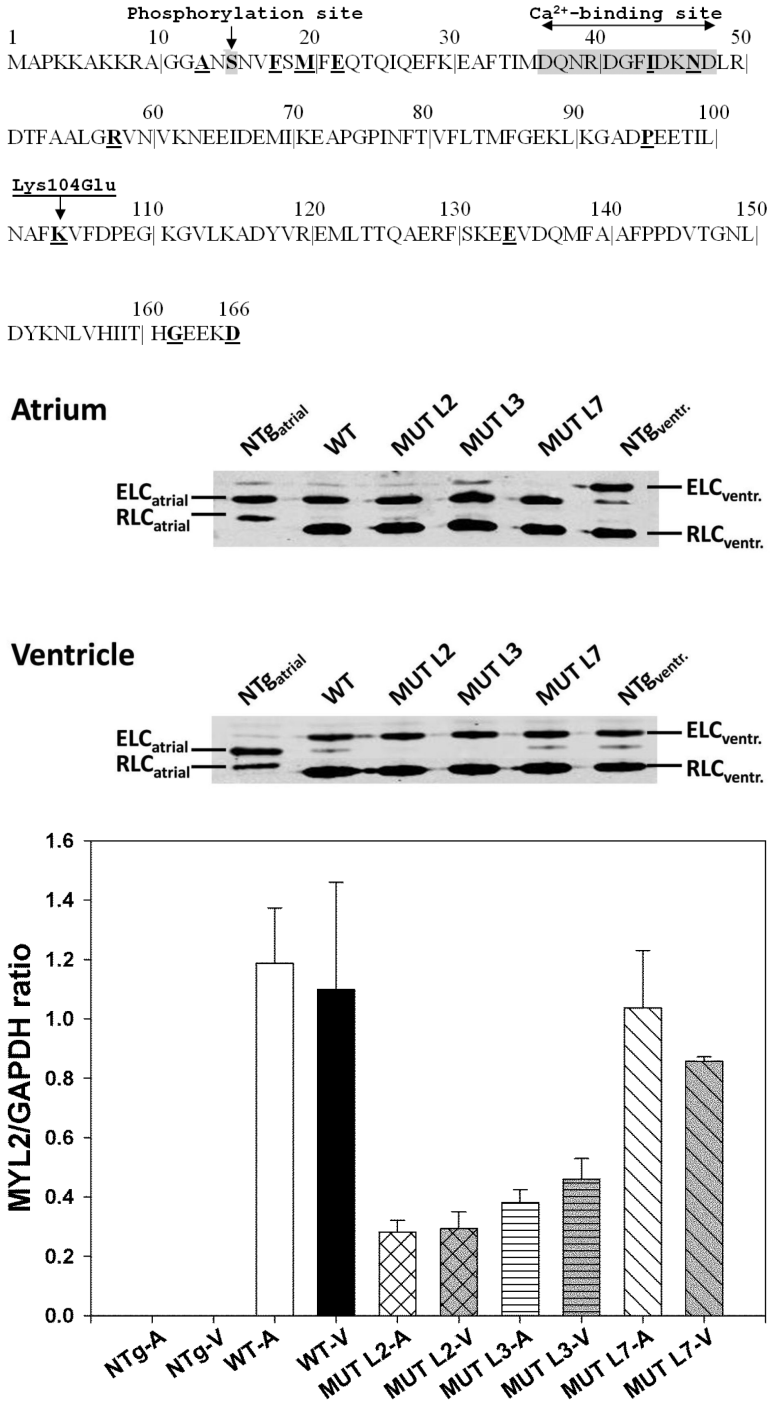

Figure 1. The Lys104Glu mutation in the human ventricular RLC expressed in transgenic mice

A. Amino acid sequence of the human ventricular myosin RLC (GenBank accession no. **P10916**) and the sites of HCM-associated mutations (underlined); also indicated the Ser15 phosphorylation site and the Ca^{2+}-binding site (shadowed). **B.** RLC-Lys104Glu expression in transgenic mice. Atrial (upper panel) and ventricular (lower panel) myofibrils from Tg-MUT L2, L3 and L7 mice were probed for protein expression: 95±2% (n=12) (L2), 97±1% (n=12) (L3) and 99±0.5% (n=12) (L7) of Lys104Glu RLC mutant were incorporated into the

hearts of Tg-MUT mice compared to 97.0±3% (n=12) of Tg-WT L2 generated previously [6]. The data are presented as average of n experiments performed on cardiac myofibrils and heart extracts ± SEM. No differences in protein expression level were observed between the preparations. Note that $RLC_{ventr.}$ migrated faster than RLC_{atrial} while no differential gel mobility was monitored between the mouse and human $RLC_{ventr.}$. Abbreviations: NTg, non-transgenic; L, mouse line; $RLC_{ventr.}$, $ELC_{ventr.}$, ventricular isoforms of RLC or ELC. **C.** Real-time PCR quantification of human *MYL2* gene expression in the atria and ventricles of Tg-WT and Tg-MUT L2, L3 and L7 mice. The results were expressed as a ratio of *MYL2* to *GAPDH* (housekeeping gene). Note that similar levels of mRNA expression were observed between atria (A) and ventricles (V) in all tested transgenic lines.

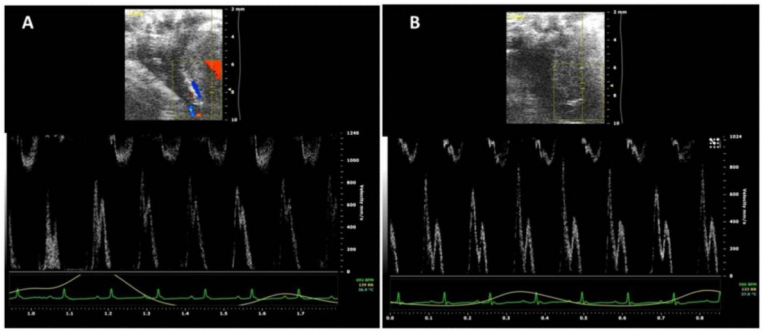

Figure 2. Representative images of mitral inflow of 6 month old Tg-MUT (A) and Tg-WT (B) mice

Notice a reduced E/A ratio in Tg-MUT compared with Tg-WT.

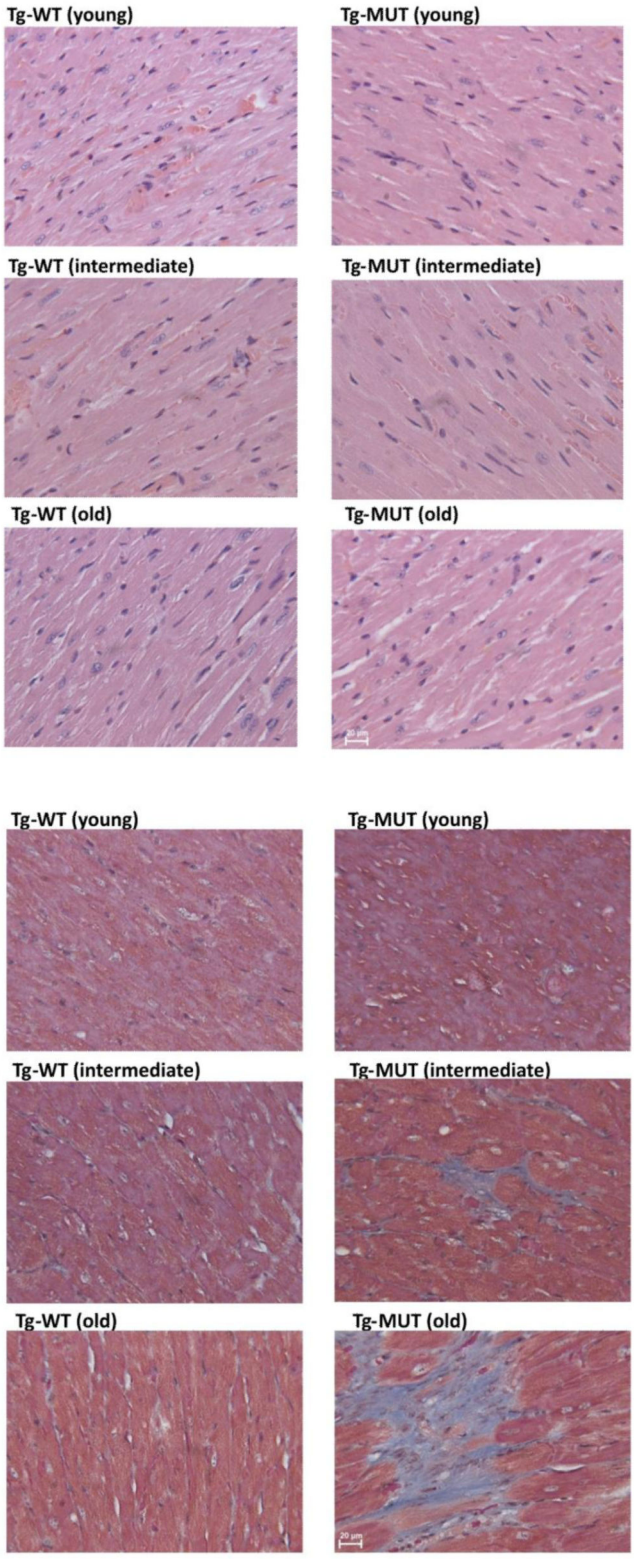

Figure 3. Histopathological assessment of left ventricular tissue from transgenic mice

A. Hematoxylin and eosin (H&E), and **B.** Masson's trichrome stained LV sections from 4.6 (young), 8.6 (intermediate) and 15.8 (old) month-old Tg-WT and 3.9 (young), 8 (intermediate) and 14.6 (old) month-old Tg-MUT mice. Note the progression of fibrosis in Tg-MUT hearts in mice of 8 to 15 months of age.

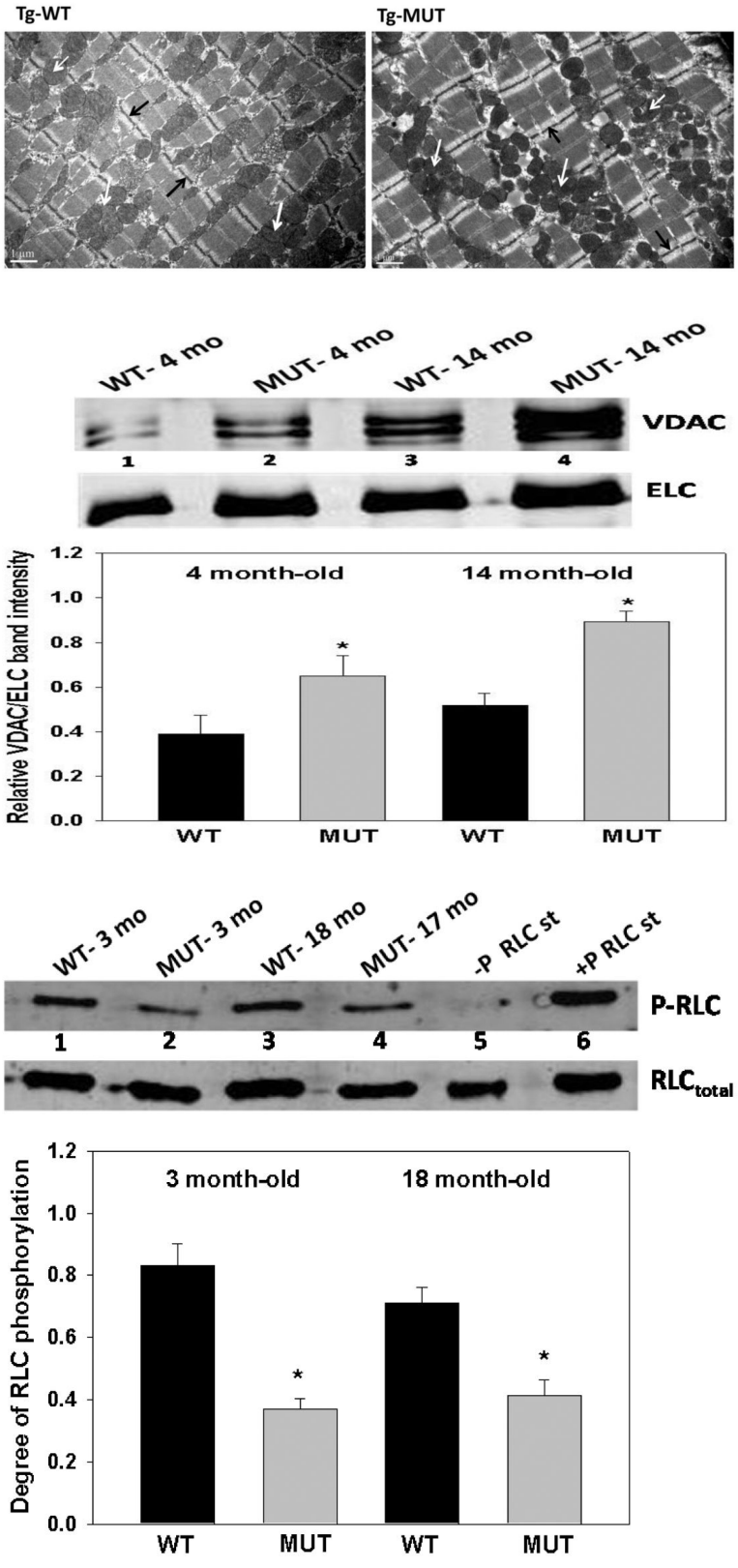

Figure 4. Mitochondrial content assessment (A, B) and analysis of protein phosphorylation (C) in the hearts of Tg-MUT vs. Tg-WT mice

A. Transmission electron micrographs showing sarcomeric ultrastructure of LV tissue from 6 month-old transgenic mice. The magnification is 10,500 X. Bar = 1 μm. Black arrows depict the Z-discs and white arrows the mitochondrial structures. Note, more mitochondria are recruited in the mutated hearts compared to WT controls. **B.** Assessment of mitochondrial content in Tg-MUT vs. Tg-WT mice. Upper panel: SDS-PAGE of heart extracts probed for VDAC (porin) protein and normalized for the myosin ELC, used as a loading control. Lanes 1 and 3, Tg-WT 4 and 14 month-old, respectively; lanes 2 and 4, Tg-MUT, 4 and 14 month-old, respectively. Lower panel: Band intensity ratios derived from gel samples run for young and old Tg-WT and Tg-MUT extracts. 14 myocardial extracts were used for each group of mice. Note that the mitochondrial content was significantly ($P<0.05$) higher in young and old Tg-MUT vs. Tg-WT hearts. **C.** Analysis of RLC phosphorylation. The level of RLC phosphorylation was determined with phospho-specific RLC antibodies and compared to the total RLC content assessed with a rabbit polyclonal RLC CT-1 antibody recognizing total RLC protein. Myofibrillar preparations from left ventricles of Tg-MUT (L2 and L3) and Tg-WT L2 mice were used. Upper panel, representative Western blot demonstrating lower RLC phosphorylation in Tg-MUT compared with Tg-WT mice. Lane 1, Tg-WT (3 month-old); lane 2, Tg-MUT (3 month-old); lane 3, Tg-WT (18 month-old); lane 4, Tg-MUT (17 month-old); lane 5: −P RLC standard protein; lane 6, +P RLC standard protein. Lower panel, quantification of RLC phosphorylation in Tg-MUT vs. Tg-WT mice. The data were collected from 13 independent Western blots. Note that young and old Tg-MUT mice showed a significantly lower level of endogenous RLC phosphorylation compared to age matched Tg-WT ($P<0.05$). Abbreviations: VDAC, Voltage-dependent anion channel; −P, unphosphorylated RLC; +P, phosphorylated RLC; L, mouse line.

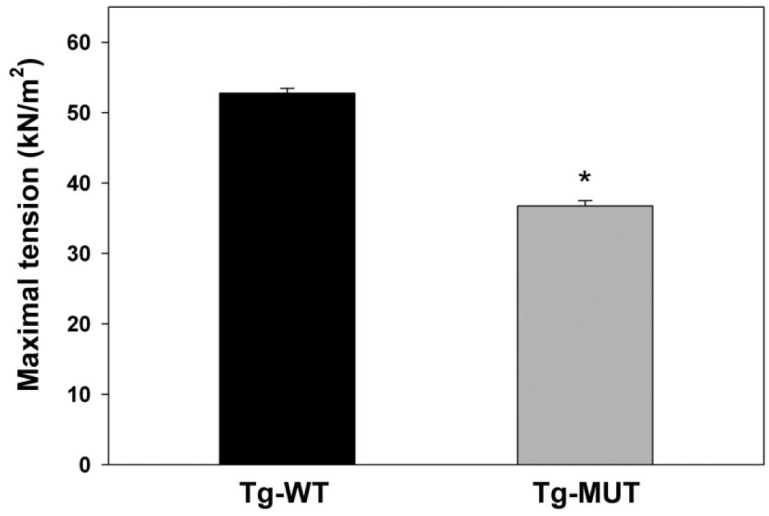

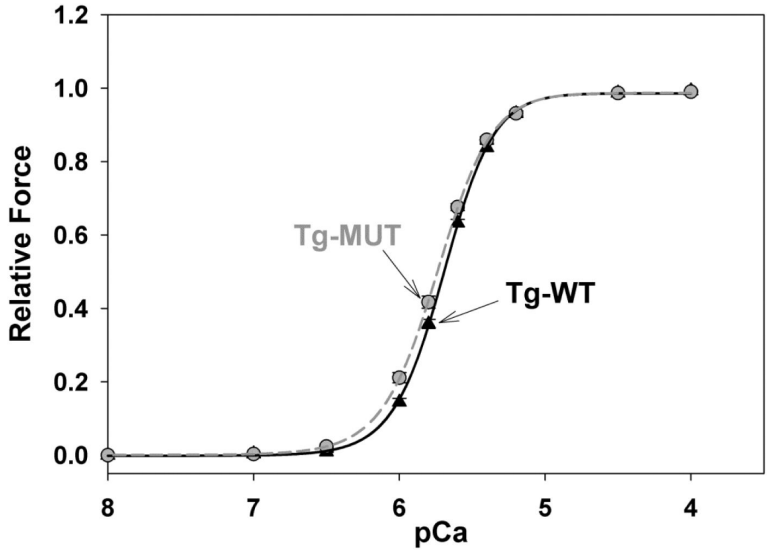

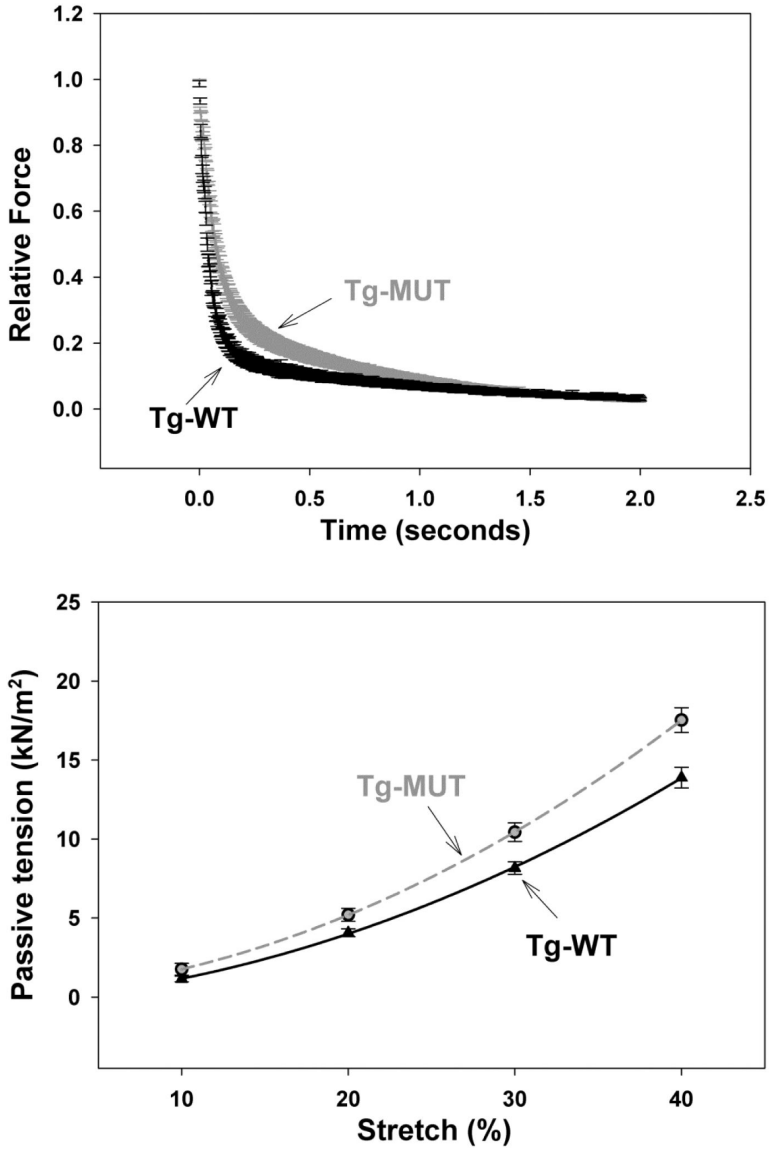

Figure 5. Steady state force (A), calcium sensitivity of force (B), muscle relaxation kinetics (C) and passive tension measurements (D) in skinned papillary muscle strips from Tg-WT and Tg-MUT mouse hearts

A. Maximal tension assessment at saturating (pCa 4) calcium concentrations. Note Tg-MUT skinned papillary muscle strips developed a 1.4-fold lower maximal force (per cross-sectional area of muscle strip) compared with Tg-WT ($P<0.01$). Error bars represent SEM. **B.** Calcium sensitivity of force in skinned papillary muscle strips from Tg-WT vs. Tg-MUT mice. No significant ($P>0.05$) changes in the Ca^{2+} sensitivity of force or Hill coefficient values were observed between the strips from Tg-MUT animals compared with Tg-WT. Error bars represent SEM. **C.** Muscle relaxation dependence in Tg-MUT and Tg-WT papillary muscle strips. A significant reduction in relaxation rates was observed in Tg-MUT vs. Tg-WT muscle strips ($P<0.01$). **D.** Assessment of passive tension (passive stiffness) under relaxation conditions (pCa 8). Error bars represent SEM. Note significantly increased

levels of passive tension in Tg-MUT compared to Tg-WT mice ($P<0.001$, as determined by ANOVA for repeated measurements).

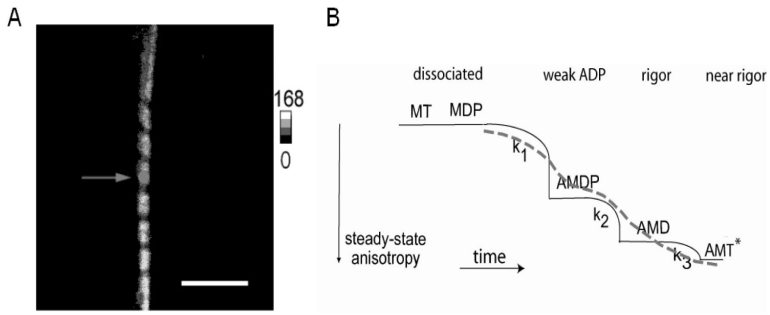

Figure 6. Fluorescence lifetime image of relaxed myofibril (A) and the 3-state model of muscle contraction (B)

A. Native myosin ELC was exchanged with 10 nM SeTau-ELC in myofibrils as described in Materials and Methods. In the image, the gray circle represents a projection of the confocal aperture on the sample plane (diameter 0.5 μm). The black and white scale is from 0 (black) to 168 (white). Scale bar = 5 μm, sarcomere length = 2.1 μm. Images were acquired on a PicoQuant Micro Time 200 confocal lifetime microscope. The sample was excited with a 640 nm pulsed laser and observed through a LP 650 nm filter. **B.** The anisotropy values associated with different cross-bridge states are 0 for MT MDP, intermediate for AMDP and maximum for AM, AMD and AMT* (rigor, strongly bound or near rigor) states. Autocorrelation function (ACF) of such a process is shown schematically as the dashed line. Abbreviations used in the 3 state model of muscle contraction: M, Myosin; D, ADP; P, inorganic phosphate; A, F-actin; T, ATP.

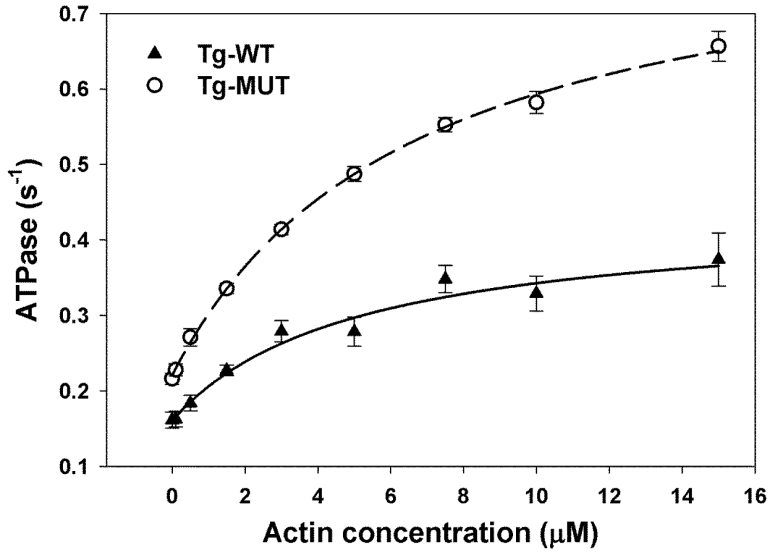

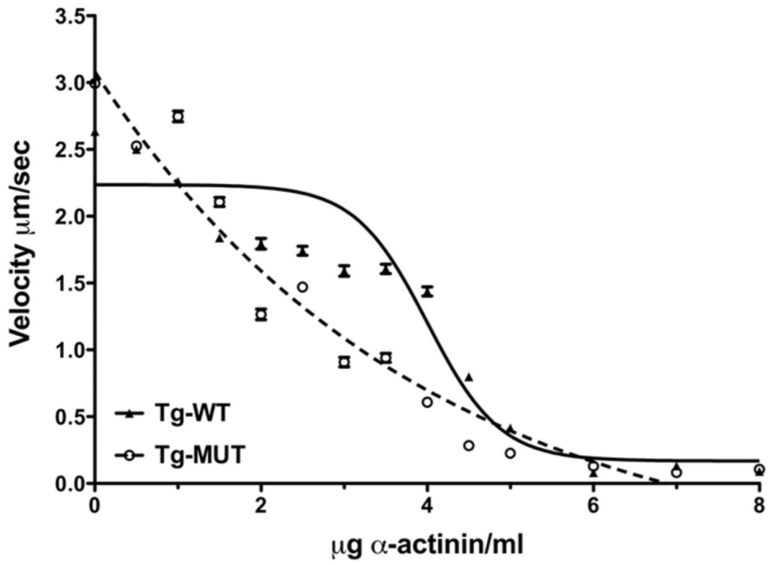

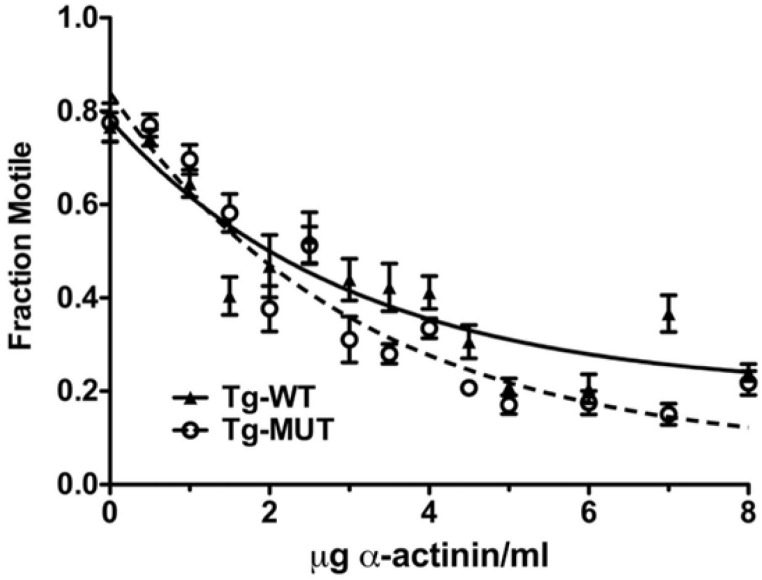

Figure 7. Actin-activated myosin ATPase activity (A), and Frictional load *in vitro* motility assays (B, C)

A Measurements were performed on myosin isolated from left and right ventricles of Tg-MUT and Tg-WT mice (6-7 hearts per preparation). ATPase assays were run in triplicate with n=16 individual measurements for WT and n=13 for Tg-MUT. Note, significant differences in V_{max} and no difference in K_m between the groups. **B.** Actin sliding velocity as a function of α-actinin concentration. Tg-MUT myosin propelled actin at a higher unloaded sliding velocity. However, once α-actinin was applied to the flow cell the velocity dropped until reaching a plateau of ~0.25 μm/s. Conversely Tg-WT myosin had a slower unloaded velocity that dropped less steeply with α-actinin concentration until ~4 μg/ml α-actinin. At higher α-actinin concentrations velocity declined to a plateau similar to Tg-MUT. **C.** Fraction motile filaments as a function of applied α-actinin. The fraction of motile filaments for both Tg-WT and Tg-MUT illustrates a similar relationship as observed for velocity in B for the mutant myosin. However, WT myosin plateaus at a higher percent filaments motile than the mutant myosin, consistent with a reduction in force generation by Tg-MUT [41]. Error bars represent SEM.

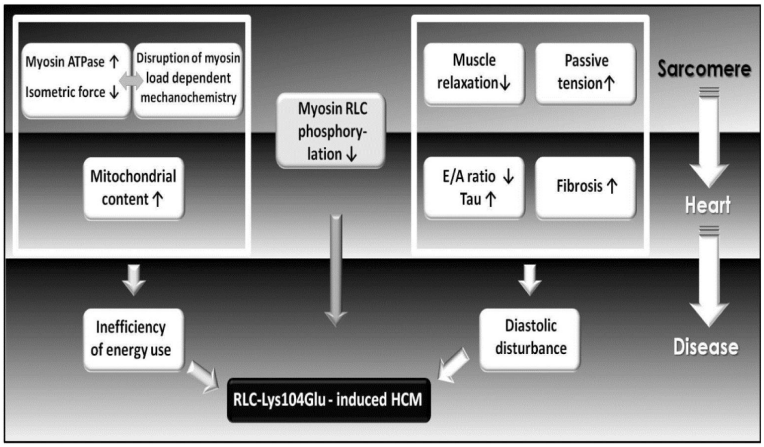

Figure 8. Integrated molecular effects of the Lys104Glu mutation in the myosin RLC depicted at the level of sarcomere and the whole heart that contribute to the development of hypertrophic cardiomyopathy (HCM) in transgenic mice

At the sarcomere level, the Lys104Glu mutation leads to a decrease in contractile force, increased maximal ATPase activity, and a decrease in muscle relaxation rate. It also results in elevated passive tension. Disruption of myosin load-dependent mechanochemistry is most likely responsible for adverse changes in force production in Tg-MUT mice. These molecular events further trigger morphological and functional remodeling of the heart manifested by abundant mitochondria, development of fibrosis and altered diastolic indices. These changes are anticipated to result in diastolic disturbance in Tg-MUT mice, which together with inefficiency in energy use and diminished RLC phosphorylation may trigger the development of Lys104Glu-RLC induced heart disease.

Table 1

Echocardiography and hemodynamic parameters in 6 month old Tg-MUT vs. Tg-WT mice

Echo/Doppler	**Tg-Lys104Glu (n=10 males)**	**Tg-WT (n=10 males)**	**P-value**
Heart Rate (bpm)	480±16	471±14	>0.05
Weight (g)	32±1.3	36±0.8	>0.05
Ant. wall (mm)	0.86±0.05	0.87±0.03	>0.05
Post. wall (mm)	0.72±0.04	0.71±0.02	>0.05
EF (%)	64±1.7	64±2.7	>0.05
Dec. time (ms)	25±2.2	21±1.8	>0.05
E/A	1.5±0.05*	1.8±0.16	0.011
E/e’	26±2	26±2	>0.05
e’ (mm/s)	−31±2	−30±2	>0.05
s’(mm/s)	27±0.9	28±1.3	>0.05
Invasive hemodynamics	**Tg-Lys104Glu** (n= 5 males)	**Tg-WT** (n= 6 males)	
dp/dtmax (mmHg/s)	9,319±613	10,840±1,244	>0.05
(dp/dtmax)/ (P@dp/dtmax) (1/s)	162.0±19.7	174.4±11.2	>0.05
PRSW (mmHg)	79.8±7.7	94.9±6.4	>0.05
dp/dtmin (mmHg/s)	−7,911±1,188	−11,024±947	0.068
Tau (ms)	7.1±1.3	4.5±0.3	0.059

Data are mean ± SEM. Abbreviations: Ant., anterior; Post., posterior; EF, Ejection Fraction; Dec., deceleration; E, early mitral inflow; A, late mitral inflow; e', early diastolic velocity; s', systolic tissue velocity; dp/dtmax, maximum derivative of LV pressure; (dp/dtmax)/(P@dp/dtmax), ratio of dp/dtmax to pressure at dp/dtmax; PRSW, Preload Recruitable Stroke Work; dp/dtmin, minimum derivative of LV pressure; tau, time constant (isovolumic relaxation time);

*, significant difference compared to Tg-WT.

Table 2

Echocardiography indices in senescent Tg-MUT vs. Tg-WT mice

	Tg-Lys104Glu	Tg-WT	P-value
Number of mice	12 (9 males)	15 (11 males)	
Body weight (g)	36.58±2.64	33.60±1.56	>0.05
Heart Rate (bpm)	406±52	483±19	>0.05
Ant. wall (mm)	1.19±0.07	0.70±0.02	<0.01
Post. wall (mm)	1.12±0.09	0.72±0.02	<0.01
LV diameter in diastole (mm)	3.65±0.13	4.22±0.10	<0.01
LV diameter in systole (mm)	2.12±0.08	2.84±0.10	<0.01
LV_{mass} (mg/g weight)	4.9±0.33	3.3±0.12	<0.01
LV_{vol}-end-diastole (μ1)	57±5	86±4	<0.01
LV_{vol}-end-systole (μ1)	15±1	33±3	<0.01
EF (%)	73.02±2.33	62.12±1.99	<0.01

Data are mean ± SEM. Abbreviations: Ant., anterior, Post., posterior; LV_{mass}, mg of LV weight divided by body weight; LV_{vol}, LV volume; LV_{vol}-end-systole, LV volume at the end of systole; EF, Ejection Fraction.